Journal of Earth Science, *Vol. 33*, *No. 3*, *p. 581–590*, *June 2022* *ISSN 1674-487X*
Printed in China
https://doi.org/10.1007/s12583-021-1588-7

Yangshan A-Type Granites in the Lower Yangtze River Belt Formed by Ridge Subduction: Radiogenic Ca and Nd Isotopic Constraints

Jianghao Bai[1,2,8], Mingxing Ling[*3], Xiaoyong Yang[4], Fang Liu[5], Huangling Gu[6], Zebin Luo[1,2,8], Xiaoyan Jiang[7], Zhaofeng Zhang[*1,5]

1. *State Key Laboratory of Isotope Geochemistry, Guangzhou Institute of Geochemistry, Chinese Academy of Sciences, Guangzhou* 510640, *China*
2. *CAS Center for Excellence in Deep Earth Science, Guangzhou* 510640, *China*
3. *State Key Laboratory of Nuclear Resources and Environment, East China University of Technology, Nanchang* 330013, *China*
4. *Key Laboratory of Crust-Mantle Materials and Environments, School of Earth and Space Sciences, University of Science and Technology of China, Hefei* 230026, *China*
5. *International Research Center for Planetary Science, College of Earth Sciences, Chengdu University of Technology, Chengdu* 610059, *China*
6. *School of City and Environment, Hunan University of Technology, Zhuzhou* 412007, *China*
7. *State Key Laboratory of Ore Deposit Geochemistry, Institute of Geochemistry, Chinese Academy of Sciences, Guiyang* 550081, *China*
8. *University of Chinese Academy of Sciences, Beijing* 100049, *China*

Jianghao Bai: https://orcid.org/0000-0002-1043-2400; Mingxing Ling: https://orcid.org/0000-0002-4859-6451; Zhaofeng Zhang: https://orcid.org/0000-0003-1797-7507

ABSTRACT: The Early Cretaceous aluminous A-type granites in the Lower Yangtze River belt (LYRB) can provide important insights into the Mesozoic magmatism in eastern China, but their origin remains highly controversial. In this study, radiogenic Ca-Nd isotopic analysis was performed for syenite porphyry and alkali-feldspar granite porphyry of the Yangshan pluton, a typical aluminous A-type granitic intrusion in the LYRB, to constrain its source and geodynamic setting. The results show that ε_{Ca}(126 Ma), ε_{Nd}(126 Ma) and K/Ca_{source} of the syenite porphyry range from -0.24 to +0.96, -7.2 to -6.0, and 0.31 to 1.26, respectively. The corresponding values for the alkali-feldspar granite porphyry range from 0.26 to 0.84, -8.0 to -6.1, and 0.79 to 1.08, respectively. Binary mixing modeling indicates that they were originated from the same sources with different proportion, namely, a mixing of 50% to 75% Neoproterozoic crust and 50% to 25% asthenospheric mantle. Together with previous works, we propose that the Early Cretaceous subduction of the ridge between the Pacific and Izanagi plates was responsible for the formation of the aluminous A-type granites in the LYRB.

KEY WORDS: Lower Yangtze River belt (LYRB), aluminous A-type granite, Yangshan pluton, radiogenic Ca-Nd isotopes, ridge subduction, geochemistry.

0 INTRODUCTION

The Early Cretaceous aluminous A-type granites distributed along the Lower Yangtze River belt (LYRB) are critical for elucidating the geodynamic mechanism in eastern China. However, their genesis remains controversial. Several petrogenesis models have been proposed, including (1) crustal anatexis with or without mixing of juvenile materials (Zhang et al., 2018; Gu et al., 2017; Xu et al., 2010); (2) mixing between asthenospheric and enriched lithospheric mantle, and subsequent crystal fractionation (Yang et al., 2017); (3) upwelling of the asthenospheric mantle for A_1-type granites, and partial melting of metasomatized lithospheric mantle for the A_2-type (Li et al., 2014, 2012, 2011); (4) metasomatized mantle for A_1-type granites, and reworking of Mesoproterozoic crust for A_2-type granites (Yan et al., 2015); (5) partial melting of residual lower continental crust (Jiang et al., 2018a; Wang et al., 2018); and (6) generation from enriched lithospheric mantle with crustal contamination (Cao et al., 2008; Du et al., 2007). One reason for the controversy on the aluminous A-type granites may be the difficulty in distinguishing the contribution of different mantle components to granitic formation based on conventional radiogenic isotopes (e.g., Sr, Nd, Pb and Hf). As an example, only radiogenic Nd isotopic data often make it difficult to discern lithospher-

*Corresponding authors: mxling@ecut.edu.cn; zzf@cdut.edu.cn

Manuscript received June 23, 2021.
Manuscript accepted October 13, 2021.

Bai Jianghao, Ling Mingxing, Yang Xiaoyong, Liu Fang, Gu Huangling, Luo Zebin, Jiang Xiaoyan, Zhang Zhaofeng, 2022. Yangshan A-Type Granites in the Lower Yangtze River Belt Formed by Ridge Subduction: Radiogenic Ca and Nd Isotopic Constraints. *Journal of Earth Science*, 33(3): 581–590. https://doi.org/10.1007/s12583-021-1588-7. http://en.earth-science.net

ic mantle from juvenile crust (Mills et al., 2018), and the inconsistent λ^{176}Lu values result in contradictory interpretation of the same Hf isotopic data (Kreissig and Elliott, 2005; Bizzarro et al., 2003; Scherer et al., 2001). To overcome this deficiency, a novel tool, radiogenic ^{40}Ca isotope, was explored in this study to provide new constraints on the petrogenesis of A-type granitic magmas.

Calcium (Ca), a major constituent element of the Earth, plays a critical role in geological processes (e.g., Lu et al., 2020; Zhu et al., 2020; Chen et al., 2018; Kang et al., 2017; Liu et al., 2017a). It has six stable isotopes, with mass number of 40, 42, 43, 44, 46, and 48, and typical natural abundances of 96.98%, 0.642%, 0.133%, 2.056%, 0.003%, and 0.182%, respectively (DePaolo, 2004). The most abundant isotope, ^{40}Ca, has both non-radiogenic and radiogenic Ca isotopic variations in terrestrial materials. The latter is the daughter product of radioactive ^{40}K. Approximately 89.5% of ^{40}K produces ^{40}Ca by β^- emission with a half-life of 1.25 Ga (DePaolo, 2004; Steiger and Jager, 1977). The short half-life of ^{40}K, relative to the age of the Earth, means that radiogenic ^{40}Ca is more sensitive to the contribution of pre-existing continental crust than other long-lived decay system such as Rb-Sr methods (the half-life of ^{87}Rb is ~49 Ga) (Mills et al., 2018; Kreissig and Elliott, 2005). Moreover, potassium (K) and Ca are strongly differentiated during the formation of continental crust (Caro et al., 2010), which would result in granite with K/Ca ratios two to four orders of magnitude higher than those of the mantle. The mantle typically has a K/Ca ratio of 0.01 (Salters and Stracke, 2004), with a ^{40}K/^{44}Ca ratio of 0.000 06, and an overall variation in ^{40}Ca/^{44}Ca ratios through geological time of 0.000 6. Simon et al. (2009) showed that the ε_{Ca} value of bulk silicate earth relative to NIST SRM 915a range from -0.68±2.28 to -0.93±0.61, suggesting that the NIST SRM 915a may possess radiogenic ^{40}Ca excesses. The similar conclusion was obtained by He et al. (2017). However, Caro et al. (2010) concluded that no resolvable difference in radiogenic Ca isotopic between the mantle and this standard were observed by measuring eight mafic rocks. Combining these data with the new (ultra)mafic rocks, Mills et al. (2018) found that the mantle is 0.7ε lower than SRM 915a.

Previous studies have also clearly demonstrated that radiogenic ^{40}Ca is a robust tracer in igneous petrogenesis (Mills et al., 2018; Marshall and DePaolo, 1989, 1982), early crust-mantle evolution (Kreissig and Elliott, 2005), the oceanic Ca cycle (Antonelli et al., 2021; Caro et al., 2010) and post-formation K depletion of the lower continental crust (Antonelli et al., 2019).

In this contribution, we report new radiogenic Ca-Nd isotopes for the aluminous A-type graintes in the LYRB, coupled with compilation of the geochemical data in literature, in order to (1) constrain the radiogenic Ca isotopic composition of the aluminous A-type graintes in the LYRB and their petrogenesis, and (2) elucidate the Early Cretaceous geodynamic evolution in the LYRB in eastern China.

1 GEOLOGICAL SETTING AND SAMPLES

The Yangtze Block lies between the Dabie-Sulu orogenic belt to the north and the Cathaysia Block to the south (Fig. 1). It comprises the Archean crystalline basement (the Kongling Group) composed of tonalitic, trondhjemitic and granitic (TTG) gneisses, metasedimentary and amphibolite rocks (Ren et al., 2020; Qiu et al., 2000; Gao et al., 1999). The basement is unconformably overlain by the Paleoproterozoic metasedimentary rocks, Cambrian to Silurian chert nodules, limestones and clastic rocks, and Devonian to Triassic sandstone, shale and argillaceous clastic rocks (Fan et al., 2016; Yan et al., 2015). The LYRB refers to the northern segment of the Yangtze Block (Fig. 1), which extends from Hubei Province in the west to the Jiangsu Province in the east (Ling et al., 2009). It primarily consists of the Late Precambrian metasedimentary and metavolcanic rocks, as well as Early Paleozoic clastic rocks, and Neoproterozoic and Mesozoic igneous rocks (Qian et al., 2019; Jiang et al., 2018b; Wu et al., 2012). In particular, Late Mesozoic igneous rocks are extensively exposed and are closely associated with polymetallic deposits (e.g., Liu G X et al., 2021; Liu S S et al., 2020), thus attracting widespread attention from geologists (Sun et al., 2010; Ling et al., 2009; Mao et al., 2006; Chen et al., 2001; Chang et al., 1991). The Mesozoic rocks were previously divided into two stages: (1) the 150 to 136 Ma rocks mainly comprise I-type granite, including granodiorite and monzagranite rocks; (2) the 136 to 120 Ma rocks consist of A-type granite and syenite as well as their volcanic counterparts (Wu et al., 2012). However, recent U-Pb, Rb-Sr and Ar-Ar ages indicate three stages: granodiorite from 152 to 136 Ma, monzogranite from 136 to 130 Ma, and K-feldspar granite from 130 to 120 Ma (Zhang et al., 2018).

The Yangshan pluton (30°17′N to 30°18′30″N, 117°42′28″E to 117°46′28″E) located in the northeast of Shitai County, Anhui Province, is a part of the Jiuhuashan Complex (Fig. 2). It is tectonically part of the Shitai dome fold, which is situated in the northern margin of the Lower Yangtze Block (Gu et al., 2017). The unit also comprises Late Neoproterozoic low-grade metasedimentary and metavolcanic rocks, and Paleozoic marine clastic sediments and carbonates (Jiang et al., 2018b; Wang, 2009). Rock types of the Yangshan pluton mainly include alkali-feldspar granite porphyry and syenite porphyry, both of which belong to aluminous A-type granites. The alkali-feldspar granite porphyry comprises phenocrysts and groundmass. The phenocrysts are comprised of quartz, K-feldspar, biotite and hornblende as well as accessory zircon and apatite, making up 40 vol.% to 50 vol.% of whole rocks. The groundmass is comprised of feldspar and quartz (Gu, 2017). The syenite porphyry is composed of 10 vol.% to 20 vol.% phenocrysts including quartz, K-feldspar, plagioclase and biotite, as well as accessory zircon and apatite (Gu, 2017).

2 ANALYTICAL METHODS

Radiogenic Ca-Nd isotopic analysis was conducted in a class 100 hood at the State Key Laboratory of Isotope Geochemistry, Guangzhou Institute of Geochemistry, Chinese Academy of Sciences (SKLaBIG-GIGCAS) and described in the following two subsections.

The separation of Ca follows the procedures described by Zhu et al. (2016) and Liu et al. (2017b) with minor modifications (Table S1). Whole rock powder samples were dissolved in a mixture of concentrated HF and HNO_3 (3 : 1) for 5 days at 120 °C. Once in solution, the samples were evaporated to dryness at 100 °C and redissolved in 2 mL of 6 M HCl to remove insoluble fluoride compounds. The samples were finally dis-

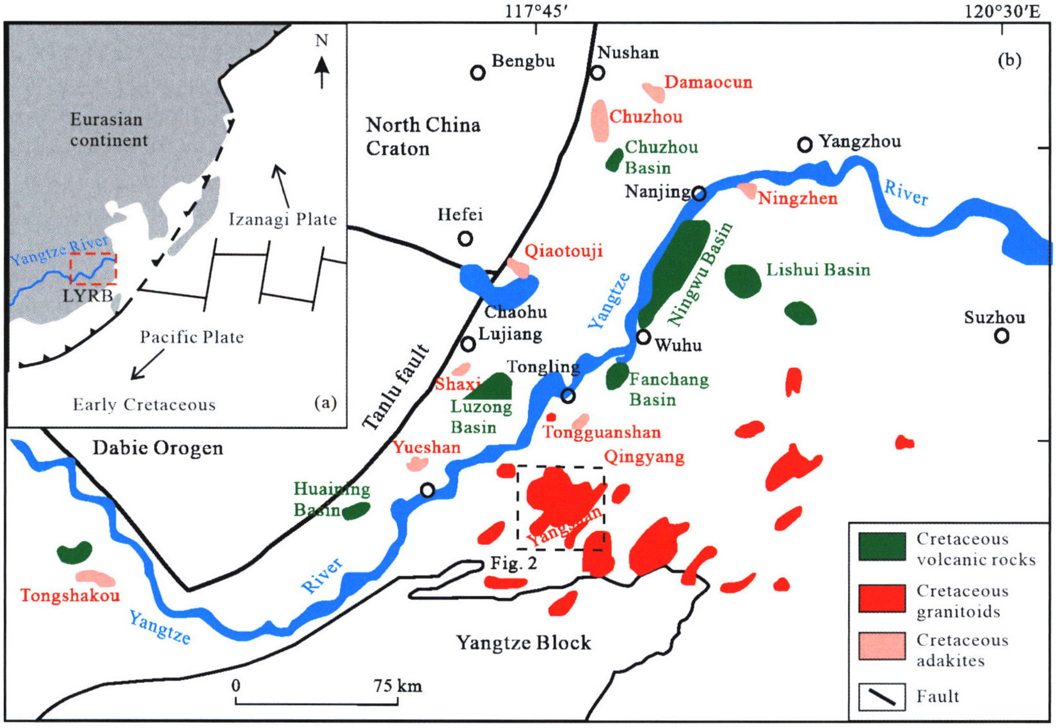

Figure 1. Geological map of the Lower Yangtze River belt. (a) Sketch map showing the ridge subduction between the Izanagi and Pacific plates; (b) geological sketch map showing the Early Cretaceous igneous rocks in the LYRB (modified after Jiang et al., 2018b; Su et al., 2013; Ling et al., 2009; Sun et al., 2007).

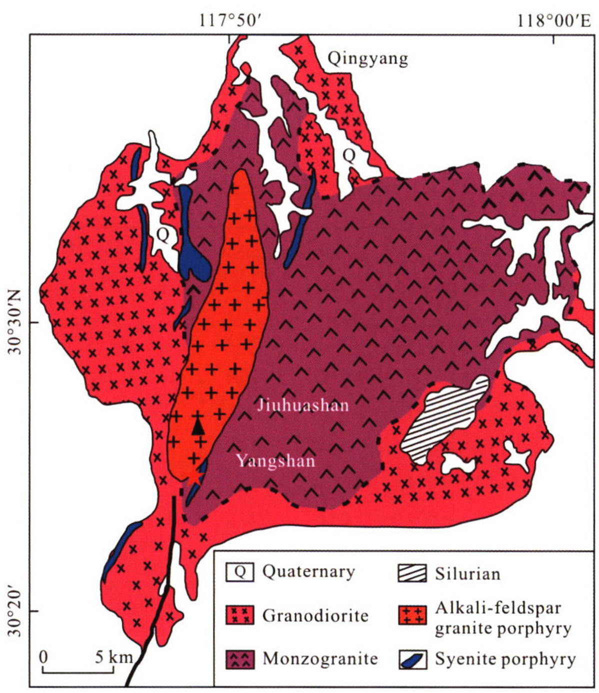

Figure 2. Geological map of the Yangshan intrusion, displaying the rock types and sample localities (modified after Jiang et al., 2018b; Gu et al., 2017; Xu et al., 2010).

solved in 0.05 mL of 1.6 M HCl to obtain a clear solution for column separation. The completely digested samples without addition of the double spike were loaded on the Teflon column containing 1 mL AG MP 50 (100 to 200 meshes) resin to purify Ca. Given that the samples analyzed here have the high K/Ca ratios (4 to 19), it is necessary to add two chemical separations as high-K samples could lead to drifting of the Ca elution peaks. In the first chemical separation, we collected solutions from 17 to 45 mL to ensure the 100% recovery of Ca. It is likely that the residual K was presented in the Ca cuts. According, 18 to 44 mL solutions in the second purification of Ca following the methods of Zhu et al. (2016) and Liu et al. (2017b) were applied to further remove residual K. Using the modified purification procedure, a perfect separation of K and Ca with nearly 100% Ca recovery for these samples was achieved well (Table S1).

Radiogenic Ca isotopic ratio was determined by thermal ionization mass spectrometry (TIMS). Purified Ca (~3 μg) was loaded on a single Ta filament with 5% phosphoric acid as an activator. A single-sequence Faraday cup of L2, C, H1, H2 and H3 was used to collect ^{40}Ca, ^{41}K, ^{42}Ca, ^{43}Ca and ^{44}Ca, simultaneously. The $^{42}Ca/^{44}Ca$ ratio of 0.312 21 was employed to calibrate the instrumental mass discrimination (Russell et al., 1987). The ^{41}K signal was monitored to correct isobaric interference of ^{40}K on ^{40}Ca using $^{40}K/^{41}K$ = 0.001 738. Two or three unspiked NIST SRM 915a were carried out per analysis batch, each bath consisting of 21 samples, to assess the stability of the instrument. Triplicate analyses were performed for each sample, and means ±2SD was reported (Table 1). The NIST SRM 915a without the double spike yields a $^{40}Ca/^{44}Ca$ ratio of 47.166 7 ± 0.004 9 (2σ, $N=7$). The radiogenic Ca isotopic ratio is reported as the $\varepsilon^{40/44}Ca$ value relative to the unspiked NIST SRM 915a.

$$\varepsilon_{Ca}=\left[\frac{\left({}^{40}Ca/{}^{44}Ca\right)_{sample}}{\left({}^{40}Ca/{}^{44}Ca\right)_{SRM\ 915a}}-1\right]\times 10\,000 \qquad (1)$$

Another method on assessing instrument stability is to measure the NIST SRM 915a and IAPSO seawater with the addition of a ^{42}Ca-^{43}Ca double spike. Their results are both consistent with our laboratory long-term standard values within the analytical uncertainty. One duplicated sample (13CZYS-07) exhibited satisfactory reproducibility within uncertainty (Table 1). The procedural blank was 23.6 ng, which is insignificant compared to the ~50 μg Ca column loadings. Additional details of Ca isotopic analysis are documented by Bai et al. (2020), Zhu et al. (2016) and Liu Y F et al. (2015).

Chemical separation of Nd follows the procedures reported by Ma et al. (2013). Approximately 200 ppb Nd solutions were measured on multi-collector inductively coupled plasma mass spectrometer (MC-ICP-MS, Nu Plasma 1700). $^{146}Nd/^{144}Nd$ = 0.721 9 was applied to correct instrumental mass fractionation, and the JNdi-1 standard was used to monitor instrument stability. Three replicate measurements of this standard were performed during sample analysis and an average $^{143}Nd/^{144}Nd$ ratios of 0.512 124 ± 0.000 025 (2σ, N = 3) was obtained (Table 1), consistent with the certified value within error. In addition, two standards, GSP-2 and JG-2, were used for quality-control purposes during sample purification, yielding $^{143}Nd/^{144}Nd$ ratios of 0.511 340 ± 0.000 004 (2σ) and 0.512 227 ± 0.000 003 (2σ), respectively (Table 1), which are agree well with published values (Weis et al., 2006). Whole-procedure blanks for Nd were <1 ng.

3 RESULTS

Whole-rock major and trace elements have been reported in Gu et al. (2017), thus we only summarize it birefly. The alkali-feldspar granite porphyry has SiO_2 from 76.3 wt.% to 77.4 wt.%, K_2O from 4.22 wt.% to 4.80 wt.%, Al_2O_3 from 11.95 wt.% to 12.26 wt.%, CaO from 0.17 wt.% to 0.97 wt.%, total REE concentrations from 118.5 ppm to 135.7 ppm, $(La/Yb)_N$ ratios from 4.9 to 5.9 and negative Eu-anomaly from 0.07 to 0.10 (Gu et al., 2017). The syenite porphyry has SiO_2, CaO, Al_2O_3, K_2O, and total REE concentrations of 74.91 wt.% to 75.58 wt.%, 0.30 wt.% to 0.58 wt.%, 12.32 wt.% to 12.53 wt.%, 4.99 wt.% to 5.85 wt.%, and 230.6 ppm to 251.7 ppm, respectively, with $(La/Yb)_N$ ratio of 7.5 to 8.2 and negative Eu-anomaly (Eu/Eu* = 0.14 to 0.17) (Gu et al., 2017).

Nd isotopic data for the Early Cretaceous Yangshan aluminous A-type granites from the LYRB are reported in Table 1. Whole rock ε_{Nd}(126 Ma) values of syenite porphyry range from -7.2 to -6.0 and those of alkali-feldspar granite porphyry are from -8.0 to -6.1, respectively, agreeing well with the literature values (Jiang et al., 2018b; Wang et al., 2018; Zhang et al., 2018; Gu et al., 2017; Wu et al., 2012; Xu et al., 2010). The ε_{Ca}(126 Ma) values for syenite porphyry and alkali-feldspar granite porphyry were first reported in this study ranging from -0.24 to +0.96 and 0.26 to 0.84, respectively (Table 1).

4 DISCUSSION

4.1 Magma Source of Aluminous A-Type Granites in the LYRB

The radiogenic Ca isotope geochemistry is still in its infancy. To better understanding the evolutionary process of radiogenic Ca isotope, we employed an evolution model of radiogenic Ca isotope in Yangtze Craton (Fig. 3). In this model, the evolutionary pathways of radiogenic Ca isotopic compositions are derived from different reservoirs with geological time. The three reservoirs with K/Ca = 0.01 in the mantle (Salters and Stracke, 2004), K/Ca = 0.05 in the basaltic lower crust (Rudnick and Gao, 2003),

Table 1 Radiogenic Ca-Nd isotopic compositions of the Yangshan aluminous A-type granites in the Lower Yangtze River belt

Samples	Age (Ma)[a]	Sm/Nd[a]	$^{143}Nd/^{144}Nd$	$\varepsilon_{Nd}(t)$	T_{2DM} (Ma)	K/Ca[a]	$^{40}Ca/^{44}Ca$[b]	$\varepsilon_{40/44Ca}$[c]	$\varepsilon_{40/44Ca}(t)$[d]	N	2SD	K/Ca_{source}
Syenite porphyry												
13CZYS-07	127	0.20	0.512 262 ± 0.000 003	-6.1	1 418	12.2	47.172 4 ± 0.004 4	1.21	0.24	3	0.93	0.78
13CZYS-07-R[e]			0.512 265 ± 0.000 003	-6.0	1 413		47.171 2	0.95	-0.01	1		
13YS-g1	127.6	0.20	0.512 222 ± 0.000 003	-6.9	1 487	4.4	47.167 2 ± 0.003 6	0.11	-0.24	3	0.76	0.35
13YS-g2	127.6	0.21	0.512 219 ± 0.000 005	-7.0	1 492	5.3	47.173 2 ± 0.004 1	1.38	0.96	3	0.86	1.26
13YS-g3	127.6	0.21	0.512 210 ± 0.000 004	-7.2	1 507	5.6	47.167 6 ± 0.004 7	0.19	-0.25	3	1.00	0.33
13YS-g4	127.6	0.20	0.512 246 ± 0.000 003	-6.4	1 445	6.0	47.169 8 ± 0.004 3	0.66	0.18	4	0.91	0.71
13YS-g5	127.6	0.19	0.512 243 ± 0.000 004	-6.4	1 440	9.8	47.168 9 ± 0.003 8	0.47	-0.31	3	0.81	0.31
13YS-g6	127.6	0.21	0.512 243 ± 0.000 004	-6.6	1 459	7.1	47.172 0 ± 0.004 9	1.12	0.56	3	1.04	0.99
Alkali-feldspar granite porphyry												
13CZYS-12	126	0.14	0.512 132 ± 0.000 001	-8.0	1 575	18.8	47.177 6 ± 0.003 7	2.31	0.84	3	0.78	1.08
13CZYS-13	126	0.13	0.512 231 ± 0.000 005	-6.1	1 416	15.9	47.173 8 ± 0.004 8	1.51	0.26	3	1.03	0.79
Neoproterozoic granitic gneiss												
14FC11	803					3.1	47.178 7 ± 0.005 1	2.54		3	1.08	
References												
JNdi-1			0.512 124 ± 0.000 025									
NIST SRM 915a							47.166 7 ± 0.004 9			8	1.03	
GSP-2			0.511 340 ± 0.000 004									
JG-2			0.512 227 ± 0.000 003									

[a]. After Gu (2017) and Liu L et al. (2015); [b]. normalized to $^{42}Ca/^{44}Ca$ = 0.312 21 using the exponential fractionation law (Russell et al., 1978); [c]. relative to unspiked NIST SRM 915a; [d]. t = 126 Ma, age-corrected values; [e]. full-procedure duplicate.

and K/Ca = 0.35 in average continental crust are assumed to have formed at 3 800 Ma ago, giving three different evolutionary pathways. From these three evolutionary pathways, it can be concluded that the higher the time-integrated K/Ca ratio, the greater enrichment in radiogenic ^{40}Ca. Moreover, this is indistinguishable radiogenic Ca compositions between lower crust and the mantle within the analytical uncertainties. Therefore, the values of $\varepsilon_{Ca} < 1$ indicate that these magma mainly involved mantle compositions in their genesis, or were generated by partial melting of mafic lower crust. The K/Ca ratios of 0.35, the highest value formed from the upper mantle, was applied to simulate the evolutionary pathways of radiogenic Ca isotopes from the Nd model age (1 500 Ma) to remelting. It is quite clear that remelting occurred at 126 Ma based on the U-Pb ages. Subsequently, the K/Ca ratio was revised to 9.5 (the average value of these samples) and evolved to the present day (green line). Another evolutionary pathway also suggests that even when highest K/Ca ratio (0.35) in crust-mantle separation was used, its results were still lower than measured data (brown line) (Fig. 3). Other evolutionary paths did not evolve to match the measurements (Fig. 3). The contradiction between theoretical and experimental studies could be best explained by changes in sources compositions, which may have added new materials to its source.

There appear to be only one published report on radiogenic Ca isotopic compositions of Dabie granitoids in China (Wang et al., 2019). The Dabie granitoids display age-corrected ε_{Ca}(126 Ma) values from 0.01 to 1.15, while the Early Cretaceous aluminous A-type granites range from -0.31 to 0.96, all of which are broadly identical to the mantle value within error (Table 1). In order to further distinguish their source compositions, we estimated source K/Ca ratio of Dabie granitoids and LYRB aluminous A-type granites using Eq. (2) and followed the method of Marshall and Depaolo (1989).

$$\left(\frac{\mathrm{K}}{\mathrm{Ca}}\right)_{\text{source}} = \frac{\varepsilon_{Ca}(T) - \varepsilon_{Ca}(T_0)}{Q_{Ca}\left(e^{\lambda_K T_0} - e^{\lambda_K T}\right)} \tag{2}$$

where

$$Q_{Ca} = \frac{R_\beta(\mathrm{Ab}\,^{40}\mathrm{K}/\mathrm{Ab}\,^{44}\mathrm{Ca})}{(^{40}\mathrm{Ca}/^{44}\mathrm{Ca})_{\text{mantle}}} \times 10\,000$$

Ab is isotopic abundance; K/Ca indicates the atomic ratio (Marshall and Depaolo, 1989); λ_K and R_β are the total decay constant of ^{40}K and the branching ratio, respectively (DePaolo, 2004; Steiger and Jager, 1977); $\varepsilon_{Ca}(T)$ and $\varepsilon_{Ca}(T_0)$ denote ε_{Ca} values the time T (zircon U-Pb age) and T_0 (Nd model age), respectively. $\varepsilon_{Ca}(T)$ can be calculated from measured ^{40}Ca/^{44}Ca, K/Ca ratios and U-Pb ages, while $\varepsilon_{Ca}(T_0)$ is -0.70 (Mills et al., 2018), assuming that the crustal reservoir derived from the upper mantle that time.

Combining Nd isotopic data with zircon U-Pb ages (Wang et al., 2019; He et al., 2013), the source K/Ca ratios could be calculated. The results show that the source K/Ca ratios (126 Ma) for Dabie granitoids range from 0.33 to 0.61 and are plotted in the lower continental crust field in an ε_{Ca}(126 Ma)-K/Ca$_{source}$(126 Ma) diagram (Fig. 4). This observation indicates that Dabie granitoids originated from the middle-lower continental crust, consistent with previous studies (He et al., 2013; Ling et al., 2011; Huang et al., 2008; Wang et al., 2007), which supports the reliability of the radiogenic Ca isotope geochemical index. Also, the source K/Ca ratios of all samples in the LYRB ranging from 0.31 to 1.26 were obtained (Table 1). It appears that the source K/Ca ratios of the LYRB samples are, on average, higher than those of the Dabie granitoids (Fig. 4), indicating that they have different source compositions. More specifically, the Early Cretaceous aluminous A-type granites source clearly has higher K/Ca materials than Dabie granitoids. In additions, the vast majority of the LYRB samples are substantially higher than that of middle-lower crust (0.1 to 0.5) (Rudnick and Gao, 2003), and tend to cluster around the value for average upper crust value (0.95) (Taylor and McLennan, 1995). Sedimentary and metasedimentary rocks are highly variable in K/Ca ratios (Marshall and DePaolo, 1982), and are lower (0.1) in the mafic lower crust (Rudnick and Gao, 2003), both of which are different from source K/Ca ratios of these samples. The ε_{Ca}(126 Ma) values of Yangshan aluminous A-type granites are consistent with the middle-lower continental crust or mantle value at our current level of analytical precision (1 ε unit), but their source K/Ca ra-

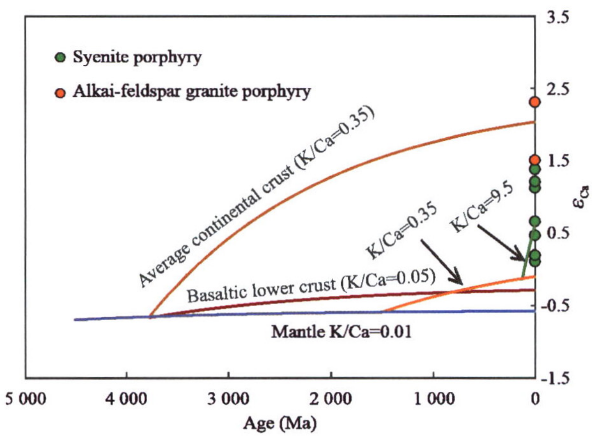

Figure 3. The evolutionary path of the radiogenic Ca isotope of the different geological reservoirs from 3 800 Ma to the present day. The oldest crustal component in the Lower Yangtze Block (Zhang et al., 2006), 3 800 Ma, was taken as the starting point. The mantle evolved throughout the geological time.

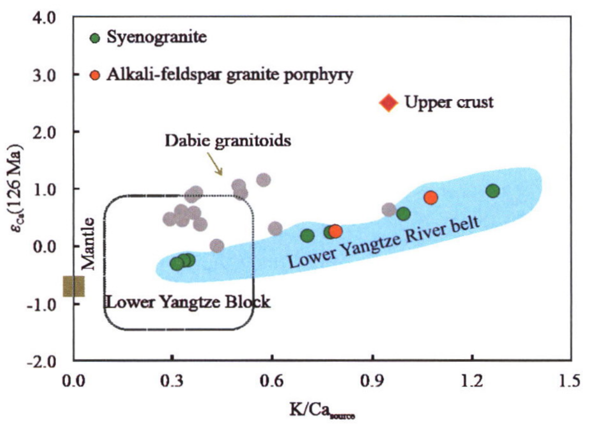

Figure 4. ε_{Ca}(126 Ma) vs. K/Ca$_{source}$ diagram (Dabie data from Wang et al. (2019), and radiogenic Ca isotopic data and K/Ca ratios from DePaolo (2004) and Rudnick and Gao (2003)). The lower continental crust field was represented by amphibolites from the Luzhenguan Complex in the Dabie-Sulu Orogen (Lu et al., 2020).

tios are substantially higher than the latter (Fig. 4), implying that their magma source may be a mixture of the upper-crust materials and mantle, rather than from the K-poor and Ca-rich mafic lower crust materials.

The extremely low radiogenic Hf and Nd isotopic compositions of the lower crust of the Yangtze Block and the relatively high aluminous A-type granites of the LYRB further suggest that the lower crustal material does not represent the main source component of aluminous A-type granites (Guo et al., 2014; Zhang and Zheng, 2013; Gao et al., 1999). Moreover, the lower continental crust has low K, Th and U contents, so rocks formed from it should have low K contents and Pb isotopic ratios, which is inconsistent with the geochemical characteristics of aluminous A-type granites in the region (Yang et al., 2017; Yan et al., 2015). Previous studies have also shown no obvious heavy rare earth elements (HREEs) differentiation, which apart from the possibility of the residues garnet in their magma source (Gu et al., 2017). The depletion of Sr and negative Eu anomalies indicate a plagioclase-rich source and reflect their shallow-crust origin (Yan et al., 2015). Zircon saturation temperatures exhibit that the formation temperature for the aluminous A-type granites in the LYRB is relatively higher (760–782 °C, with average of 772 °C) than that of the early I-type granites (667–720 °C with average of 694 °C) (Wang et al., 2018; Gu et al., 2017; Yan et al., 2015).

Thus on balance, traditional geochemical signatures and the new radiogenic ^{40}Ca data with the source K/Ca ratio (126 Ma) are best explained by a mixing of the mantle and upper crustal materials in the source of aluminous A-type granites, rather than by simple crust or mantle composition alone.

4.2 Assessing Crustal and Mantle Contributions in Aluminous A-Type Granites

To quantitatively evaluate the relative contributions of the crustal and mantle materials, a two end-member mixing model using the radiogenic ^{40}Ca and Nd isotopic for aluminous A-type granites was developed in this study. In these modeling calculations, the melts of asthenospheric mantle, the melts of lithospheric mantle, the Archean crust and Neoproterozoic crust were used as isotopic end-members (Fig. 5). The ε_{Ca} values and CaO contents for the melt derived asthenospheric and lithospheric mantle both do not differ, being -0.7ε and 11.3 wt.% (Mills et al., 2018; Hofmann, 1988), respectively. The ε_{Nd} values and Nd contents for the asthenospheric melts are +10 and 11 ppm, respectively (Chen et al., 1994; Hofmann, 1988), while the lithospheric melts are -6 and 35 ppm (Yan et al., 2015, 2005), respectively. Among the crustal end-members, the Archean crust was represented by the Kongling Group in the Yangtze Block with a CaO content of 9.59 wt.%, the ε_{Nd} values of -28, and the Nd concentration of 39 ppm (Rudnick and Gao, 2003; Gao et al., 1999). No radiogenic ^{40}Ca data have been reported for the Archean Kongling Group, but its ε_{Ca} value should be difficult to discern within the current precision range because of its low K/Ca ratio of 0.05. This conclusion is also supported by ε_{Ca} value for granitoids in the Dabie Orogen (Wang et al., 2019), which are considered as derived from ancient lower crust. In this view, an estimated ε_{Ca} value for the Archean Kongling Group of 1 was used. Neoproterozoic crust is represented by the Fuchashan Complex in southern Anhui Province with CaO and Nd contents of 3.59 wt.% and 27 ppm (Liu L et al., 2015), and an ε_{Ca}(126 Ma) value of 2.54 measured here, respectively. Modeling calculations using the above parameters indicate that the magmatic source for the aluminous A-type granites of the LYRB is composed of 50% to 75% Neoproterozoic crust and 50% to 25% asthenospheric mantle materials (Fig. 5).

In summary, we consider that the mantle compositions are important in the petrogenesis of aluminous A-type granites of the LYRB. It not only provides an indispensable heat source for the melting of the upper continental crust, but also injects materials into their magma source. Binary mixing model using

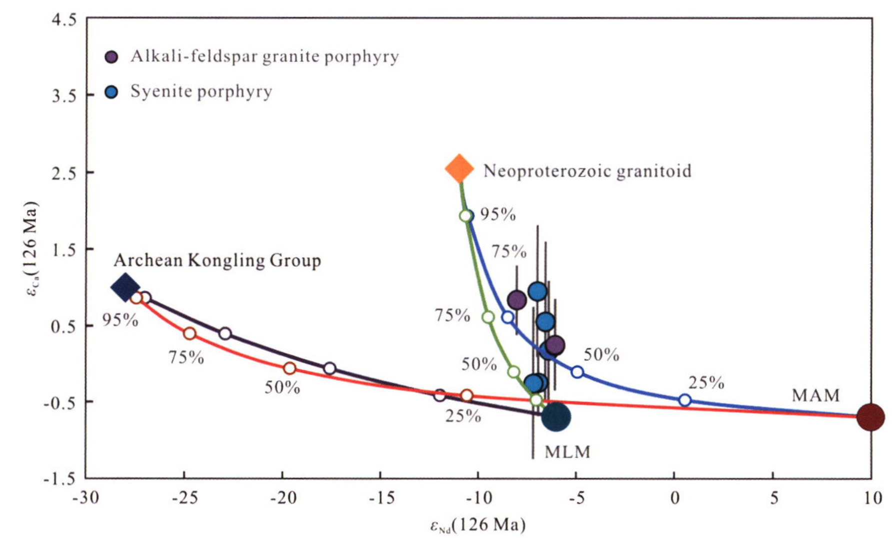

Figure 5. ε_{Ca}(126 Ma) vs. ε_{Nd}(126 Ma) diagram for the four end members mixing models. MAM is the melts of asthenospheric mantle: Nd = 11 ppm; ε_{Nd} = +10; CaO = 11.3 wt.%; ε_{Ca} = -0.7 (Mills et al., 2018; Chen et al., 1994; Hofmann, 1988). MLM is the melts of lithospheric mantle: Nd = 35 ppm; ε_{Nd} = -6; CaO = 11.3 wt.%; ε_{Ca} = -0.7 (Mills et al., 2018; Yan et al., 2015, 2005). The Archean crust was represented by the Kongling Group: Nd = 39 ppm; ε_{Nd} = -28; CaO = 9.59 wt.%; ε_{Ca} = 1 (Rudnick and Gao, 2003; Gao et al., 1999). Neoproterozoic crust was represented by Neoproterozoic granitoid: Nd = 27 ppm; ε_{Nd} = -11; CaO = 3.56 wt.% (Liu L et al., 2015), and ε_{Ca}(126 Ma) = 2.54 (Table 1).

radiogenic Ca-Nd isotopes show that a mixture of 50% to 75% Neoproterozoic crust and 50% to 25% asthenospheric mantle constitutes the main source compositions of the aluminous A-type granites in the LYRB.

4.3 Geodynamic Setting

The geodynamic setting of Mesozoic igneous rocks in the LYRB remains controversial, and several genetic models have been recommended by previous researches, as follow: (1) lithospheric thinning trigged by delamination or thermodynamic erosion (Su et al., 2013; Li et al., 2009; Xue et al., 2009; Xie et al., 2008); (2) the low angle subduction of paleo-Pacific Plate and subsequent roll-back of basaltic slab, resulting in the partial melting of the lower crust (Wang et al., 2018), or Neoproterozoic crust (Gu et al., 2017; Yang et al., 2017; Yan et al., 2015) or highly fractional crystallization (Fan et al., 2016); (3) slab tearing induced by changes in the subduction angle of paleo-Pacific Plate (Wu et al., 2012); and (4) the ridge subduction between the Pacific and Izanagi plates during the Early Cretaceous (Zhang et al., 2020; Jiang et al., 2018b; Sun et al., 2018, 2010, 2007; Ling et al., 2011, 2009). Although the geodynamic evolution of the Early Cretaceous cannot be unambiguously elucidated through the current isotopic data of the LYRB Mesozoic igneous rocks, it is clear that the unradiogenic mantle-like ε_{Ca}(126 Ma) values and upper crust-like source K/Ca ratios of the aluminous A-type granites can provide more details for the ridge subduction model.

Based on geological, geochemical, and geophysical evidence, Ling et al. (2009) proposed a ridge subduction model for the Mesozoic mineralization in the LYRB (Fig. 6). This model states that between 140 to 125 Ma, the Pacific Plate drifted southwestward and the Izanagi Plate drifted northwestward, resulting in ridge subduction. This model is favorable for the spatial distribution of adakitic and calc-alkaline rocks, Nb-enriched basalts, A-type granitoids, and ore deposits in the LYRB (Ling et al., 2009). During ridge subduction, oceanic crust near the mid-ocean ridge was hot and partially melted. As the melts ascended, they reacted with mantle peridotites and subsequent contaminated by the lower continental crust materials, forming the adakitic rocks. Oceanic crust away from the mid-ocean ridge is cold and has a high water content, which can cause dehydration of subducted slabs and generate calc-alkaline magmas. These processes clearly expound the origin of magmatic rocks in the LYRB between 150 and 136 Ma. The slab window opened and induced the upwelling of hot asthenosphere. The Nb-rich fluid released by the subducting slab led to partial melting of the metasomatized mantle, producing basaltic magma (Ling et al., 2009; Sun et al., 2008). A portion of basaltic magma rose and erupted to the surface, resulting in the formation Nb-rich basalts, while another portion intruded the crust-mantle boundary, inducing partial melting of the lower crustal materials (Fig. 6). The mixing of basaltic magma and lower crustal melts produced the intermediate-acid intrusive rocks. Besides, partial melting of the lithospheric mantle and lower continental crust led to the crustal thinning in narrow regions, creating cracks that as channels for magma to rise. Finally, the rise of hot asthenospheric melts into the shallow crustal levels induced partial melting of Neoproterozoic crust. Therefore, we propose that the series of geological processes described above controlled the formation of aluminous A-type granites in the LYRB.

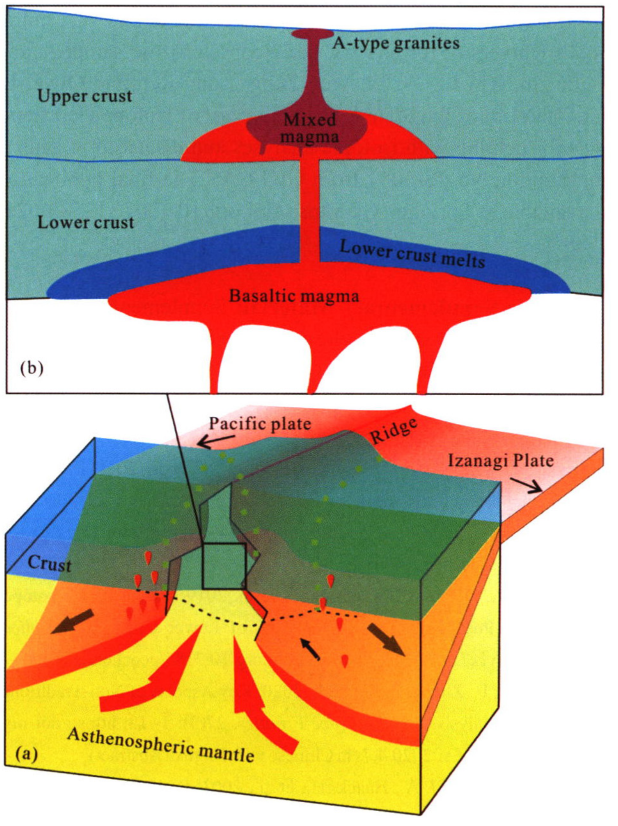

Figure 6. A simplified petrogenetic model of the Early Cretaceous aluminous A-type granites in the LYRB. (a) Modified after Luo et al. (2018), Jiang et al. (2018a) and Ling et al. (2009).

5 CONCLUSIONS

Radiogenic Ca isotope has the potential to distinguish the contribution of the mantle to granitic formation. The initial ε_{Ca}(126 Ma) values for both syenite porphyry and alkali-feldspar granite porphyry in the Yangshan pluton range from -0.31 to 0.96, consistent with the mantle within error. In conjunction with the source K/Ca ratios, the results indicate that the parental magmas of these rocks are the result of crust-mantle interactions. Binary mixing model using radiogenic Ca-Nd isotopic compositions shows that a mixture of 50% to 75% Neoproterozoic crust and 50% to 25% asthenospheric mantle materials constitutes their magma sources. Integrating with previous works, we propose that Early Cretaceous ridge subduction of the Pacific and Izanagi plates was responsible for generation of aluminous A-type granites in the LYRB.

ACKNOWLEDGMENTS

This study was supported by the Jiangxi Double Thousand Plan, the State Key Laboratory of Nuclear Resources and Environment, East China University of Technology, Nanchang (No. 2020Z03), the National Key R & D Program of China (Nos. 2016YFC0600408, 2019YFA0708400), the Strategic Priority Research Program of the Chinese Academy of Sciences (No. XDB41020102). The authors are extremely grateful to the two anonymous reviewers, whose constructive comments greatly improved the manuscript. Thanks also go to Lei Liu of Central South University for sharing the Neoproterozoic samples, and Yajun An, Xin Li, Jie Li, Wen Zeng, Long Ren and Qiwei Li and Xiao Liu of the State Key Laboratory of Isotope Geochemistry for helping with isotopic analyses and discussions. This is contribution No. IS-3081 from GIG-CAS.The final publication is available at Springer via https://doi.org/10.1007/s12583-021-1588-7.

Electronic Supplementary Material: Supplementary material (Table S1) is available in the online version of this article at https://doi.org/10.1007/s12583-021-1588-7.

REFERENCES CITED

Antonelli, M. A., DePaolo, D. J., Christensen, J. N., et al., 2021. Radiogenic ^{40}Ca in Seawater: Implications for Modern and Ancient Ca Cycles. *ACS Earth and Space Chemistry*, 5(9): 2481–2492. https://doi. org/10.1021/acsearthspacechem.1c00179

Antonelli, M.A., DePaolo, D. J., Chacko, T., et al., 2019. Radiogenic Ca Isotopes Confirm Post-Formation K Depletion of Lower Crust. *Geochemical Perspectives Letters*, 43–48. https://doi.org/10.7185/geochemlet.1904

Bai, J. H., Liu, F., Zhang, Z. F., et al., 2020. Key Aspects of Non-Traditional Isotope Analysis. *Earth Science Fronties*, 27(3): 1–13. https://doi. org/10.13745/j.esf.sf.2020.4.7 (in Chinese with English Abstract)

Bizzarro, M., Baker, J. A., Haack, H., et al., 2003. Early History of Earth's Crust-Mantle System Inferred from Hafnium Isotopes in Chondrites. *Nature*, 421(6926): 931–933. https://doi.org/10.1038/nature01421

Cao, Y., Du, Y. S., Cai, C. L., et al., 2008. Mesozoic A-Type Granitoids and Xenoliths in the Lujiang-Zongyang Area, Anhui Province: Significance in Post-Collisional Magmatic Evolution. *Geological Journal of China Universities*, 14(4): 565–576 (in Chinese with English Abstract)

Caro, G., Papanastassiou, D. A., Wasserburg, G. J., 2010. ^{40}K-^{40}Ca Isotopic Constraints on the Oceanic Calcium Cycle. *Earth and Planetary Science Letters*, 296(1/2): 124–132. https://doi.org/10.1016/j.epsl.2010.05.001

Chang, Y. F., 1991. The Copper-Iron Belt of the Lower and Middle Reaches of the Changjiang River. In: Liu, X. P., Wu, Y. C., eds., Geological Publishing House, Beijing. 379 (in Chinese)

Chen, C. F., Liu, Y. S., Feng, L. P., et al., 2018. Calcium Isotope Evidence for Subduction-Enriched Lithospheric Mantle under the Northern North China Craton. *Geochimica et Cosmochimica Acta*, 238: 55–67. https://doi.org/10.1016/j.gca.2018.06.038

Chen, D. G., Zhi, X. C., Li, B. X., 1994. The Nd, Sr and Pb Isotopic Characteristics of Lherzolite Xenoliths from Panshishan. *Geochimica*, 23(3): 245–253. https://doi.org/10.19700/j.0379-1726.1994.03.004 (in chinese with English Abstract)

Chen, J. F., Yan, J., Xie, Z., et al., 2001. Nd and Sr Isotopic Compositions of Igneous Rocks from the Lower Yangtze Region in Eastern China: Constraints on Sources. *Physics and Chemistry of the Earth, Part A: Solid Earth and Geodesy*, 26(9/10): 719–731. https://doi.org/10.1016/s1464-1895(01)00122-3

DePaolo, D. J., 2004. Calcium Isotopic Variations Produced by Biological, Kinetic, Radiogenic and Nucleosynthetic Processes. In: Johnson, C. M., Beard, B. L., Albarède, F., et al., eds., Geochemistry of Non-Traditional Stable Isotopes. De Gruyter. 55(8): 255–288. https://doi. org/10.1515/9781501509360-011

Du, Y. S., Cao, Y., Yuan, W. M., et al., 2007. Mesozoic Post-Collisional to Postorogenic Magmatic Activities and Crustal Interaction with Mantle along the Yangtze River, Anhui Provience: Evidence from Volcanic-intrusive Complexes and Xenolith. *Acta Petrologica Sinica*, 23(6): 1294–1302 (in Chinese with English Abstract)

Fan, Y., Zhou, T. F., Zhang, D. Y., et al., 2016. Genesis of the Qingyang-Jiuhuashan Complex Pluton in South Anhui Province and Its Geological Significance. *Acta Petrologica Sinica*, 32(2): 419–438 (in Chinese with English Abstract)

Gao, S., Ling, W. L., Qiu, Y. M., et al., 1999. Contrasting Geochemical and Sm-Nd Isotopic Compositions of Archean Metasediments from the Kongling High-Grade Terrain of the Yangtze Craton: Evidence for Cratonic Evolution and Redistribution of REE during Crustal Anatexis. *Geochimica et Cosmochimica Acta*, 63(13/14): 2071–2088. https://doi. org/10.1016/s0016-7037(99)00153-2

Gu, H. L., Yang, X. Y., Deng, J. H., et al., 2017. Geochemical and Zircon U-Pb Geochronological Study of the Yangshan A-Type Granite: Insights into the Geological Evolution in South Anhui, Eastern Jiangnan Orogen. *Lithos*, 284/285: 156–170. https://doi.org/10.1016/j.lithos.2017.04.007

Gu, H. L., 2017. The Yanshanian Magmatism and Its Relations to the Cu(Mo)-Au Mineralization in Guichi district, Lower Yangtze River Metallogenic Belt: [Dissertation]. Univeristy of Science and Technology of China, Hefei. 136 (in Chinese with English Abstract)

Guo, J. L., Gao, S., Wu, Y. B., et al., 2014. 3.45 Ga Granitic Gneisses from the Yangtze Craton, South China: Implications for Early Archean Crustal Growth. *Precambrian Research*, 242: 82–95. https://doi.org/10.1016/j. precamres.2013.12.018

He, Y. S., Li, S. G., Hoefs, J., et al., 2013. Sr-Nd-Pb Isotopic Compositions of Early Cretaceous Granitoids from the Dabie Orogen: Constraints on the Recycled Lower Continental Crust. *Lithos*, 156–159: 204–217. https://doi. org/10.1016/j.lithos.2012.10.011

He, Y. S., Wang, Y., Zhu, C. W., et al., 2017. Mass-Independent and Mass-Dependent Ca Isotopic Compositions of Thirteen Geological Reference Materials Measured by Thermal Ionisation Mass Spectrometry. *Geostandards and Geoanalytical Research*, 41(2): 283–302. https://doi.org/10.1111/ggr.12153

Hofmann, A. W., 1988. Chemical Differentiation of the Earth: The Relationship between Mantle, Continental Crust, and Oceanic Crust. *Earth and Planetary Science Letters*, 90(3): 297–314. https://doi.org/10.1016/0012-821x(88)90132-x

Huang, F., Li, S. G., Dong, F., et al., 2008. High-Mg Adakitic Rocks in the Dabie Orogen, Central China: Implications for Foundering Mechanism of Lower Continental Crust. *Chemical Geology*, 255(1/2): 1–13. https://doi.org/10.1016/j.chemgeo.2008.02.014

Jiang, X. Y., Li, H., Ding, X., et al., 2018a. Formation of A-Type Granites in the Lower Yangtze River Belt: A Perspective from Apatite Geochemistry. *Lithos*, 304–307: 125–134. https://doi.org/10.1016/j.lithos.2018.02.005

Jiang, X. Y., Luo, J. C., Guo, J., et al., 2018b. Geochemistry of I- and A-Type Granites of the Qingyang-Jiuhuashan Complex, Eastern China: Insights into Early Cretaceous Multistage Magmatism. *Lithos*, 316/317: 278–294. https://doi.org/10.1016/j.lithos.2018.07.025

Kang, J. T., Ionov, D. A., Liu, F., et al., 2017. Calcium Isotopic Fractionation in Mantle Peridotites by Melting and Metasomatism and Ca Isotope Composition of the Bulk Silicate Earth. *Earth and Planetary Science Letters*, 474: 128–137. https://doi.org/10.1016/j.epsl.2017.05.035

Kreissig, K., Elliott, T., 2005. Ca Isotope Fingerprints of Early Crust-Mantle Evolution. *Geochimica et Cosmochimica Acta*, 69(1): 165–176. https://doi.org/10.1016/j.gca.2004.06.026

Li, H., Zhang, H., Ling, M. X., et al., 2011. Geochemical and Zircon U-Pb Study of the Huangmeijian A-Type Granite: Implications for Geological Evolution of the Lower Yangtze River Belt. *International Geology*

Review, 53(5/6): 499 – 525. https://doi. org/10.1080/00206814.2010. 496202

Li, H., Ling, M. X., Li, C. Y., et al., 2012. A-Type Granite Belts of Two Chemical Subgroups in Central Eastern China: Indication of Ridge Subduction. *Lithos*, 150: 26–36. https://doi.org/10.1016/j.lithos.2011.09.021

Li, H., Ling, M. X., Ding, X., et al., 2014. The Geochemical Characteristics of Haiyang A-Type Granite Complex in Shandong, Eastern China. *Lithos*, 200/201: 142–156. https://doi.org/10.1016/j.lithos.2014.04.014

Li, J. W., Zhao, X. F., Zhou, M. F., et al., 2009. Late Mesozoic Magmatism from the Daye Region, Eastern China: U-Pb Ages, Petrogenesis, and Geodynamic Implications. *Contributions to Mineralogy and Petrology*, 157(3): 383–409. https://doi.org/10.1007/s00410-008-0341-x

Ling, M. X., Wang, F. Y., Ding, X., et al., 2011. Different Origins of Adakites from the Dabie Mountains and the Lower Yangtze River Belt, Eastern China: Geochemical Constraints. *International Geology Review*, 53(5/6): 727–740. https://doi.org/10.1080/00206814.2010.482349

Ling, M. X., Wang, F. Y., Ding, X., et al., 2009. Cretaceous Ridge Subduction along the Lower Yangtze River Belt, Eastern China. *Economic Geology*, 104(2): 303–321. https://doi.org/10.2113/gsecongeo.104.2.303

Liu, F., Li, X., Wang, G. Q., et al., 2017a. Marine Carbonate Component in the Mantle beneath the Southeastern Tibetan Plateau: Evidence from Magnesium and Calcium Isotopes. *Journal of Geophysical Research: Solid Earth*, 122(12): 9729–9744. https://doi.org/10.1002/2017jb014206

Liu, F., Zhu, H. L., Li, X., et al., 2017b. Calcium Isotopic Fractionation and Compositions of Geochemical Reference Materials. *Geostandards and Geoanalytical Research*, 41(4): 675 – 688. https://doi. org/10.1111/ggr.12172

Liu, G. X., Deng, Y. F., Yuan, F., et al., 2021. Rb-Sr Dating and S-Sr-Nd Isotopic Constraints on the Genesis of the Hehuashan Pb-Zn Deposit in the Middle-Lower Yangtze River Metallogenic Belt, China. *Solid Earth Sciences*, 6(2): 57–69. https://doi.org/10.1016/j.sesci.2021.04.003

Liu, L., Yang, X. Y., Santosh, M., et al., 2015. Neoproterozoic Intraplate Crustal Accretion on the Northern Margin of the Yangtze Block: Evidence from Geochemistry, Zircon SHRIMP U-Pb Dating and Hf Isotopes from the Fuchashan Complex. *Precambrian Research*, 268: 97–114. https://doi.org/10.1016/j.precamres.2015.07.004

Liu, S. S., Yang, X. Y., Chen, L. J., et al., 2020. Geological and Geochemical Characteristics and Genesis of the Cishan Gold Deposit in Tongling Ore Cluster Area, Anhui Province. *Solid Earth Sciences*, 5(3): 182–201. https://doi.org/10.1016/j.sesci.2020.06.003

Liu, Y. F., Zhu, H. L., Liu, F., et al., 2015. Methodological Study of Chemical Separation of Calcium for TIMS Measurements. *Geochimica*, 44(5): 469–476. https://doi.org/10.19700/j.0379-1726.2015.05.006 (in Chinese with English Abstract)

Lu, W. N., He, Y. S., Wang, Y., et al., 2020. Behavior of Calcium Isotopes during Continental Subduction Recorded in Meta-Basaltic Rocks. *Geochimica et Cosmochimica Acta*, 278: 392 – 404. https://doi. org/10.1016/j.gca.2019.09.027

Luo, Z. B., Xue, S., Zhang, L. P., et al., 2018. Origin of Early Cretaceous Guandian Adakitic Pluton in Central Eastern China: Partial Melting of Delaminated Lower Continental Crust Triggered by Ridge Subduction. *International Geology Review*, 60(11–14): 1707–1720. https://doi.org/10.1080/00206814.2017.1393777

Ma, J. L., Wei, G. J., Liu, Y., et al., 2013. Precise Measurement of Stable Neodymium Isotopes of Geological Materials by Using MC-ICP-MS. *Journal of Analytical Atomic Spectrometry*, 28(12): 1926–1931. https://doi.org/10.1039/c3ja50229e

Mao, J. W., Wang, Y. T., Lehmann, B., et al., 2006. Molybdenite Re-Os and Albite $^{40}Ar/^{39}Ar$ Dating of Cu-Au-Mo and Magnetite Porphyry Systems in the Yangtze River Valley and Metallogenic Implications. *Ore Geology Reviews*, 29(3/4): 307 – 324. https://doi. org/10.1016/j.oregeorev.2005.11.001

Marshall, B. D., DePaolo, D. J., 1982. Precise Age Determinations and Petrogenetic Studies Using the K-Ca Method. *Geochimica et Cosmochimica Acta*, 46(12): 2537–2545. https://doi.org/10.1016/0016-7037(82)90376-3

Marshall, B. D., DePaolo, D. J., 1989. Calcium Isotopes in Igneous Rocks and the Origin of Granite. *Geochimica et Cosmochimica Acta*, 53(4): 917–922. https://doi.org/10.1016/0016-7037(89)90036-7

Mills, R. D., Simon, J. I., DePaolo, D. J., 2018. Calcium and Neodymium Radiogenic Isotopes of Igneous Rocks: Tracing Crustal Contributions in Felsic Magmas Related to Super-Eruptions and Continental Rifting. *Earth and Planetary Science Letters*, 495: 242 – 250. https://doi. org/10.1016/j.epsl.2018.05.017

Qian, L., Wang, Y., Xie, J. C., et al., 2019. The Late Mesozoic Granodiorite and Polymetallic Mineralization in Southern Anhui Province, China: A Perspective from Apatite Geochemistry. *Solid Earth Sciences*, 4(4): 178–189. https://doi.org/10.1016/j.sesci.2019.11.006

Qiu, Y. M., Gao, S., McNaughton, N. J., et al., 2000. First Evidence of >3.2 Ga Continental Crust in the Yangtze Craton of South China and Its Implications for Archean Crustal Evolution and Phanerozoic Tectonics. *Geology*, 28(1): 11 – 14. https://doi. org/10.1130/0091-7613(2000)028011:feogcc>2.0.co;2

Ren, L., Bao, Z. W., Huang, W. T., et al., 2020. Flat-Slab Subduction and Formation of "Intraplate" Porphyry Deposits: Insights from the Jurassic High and Low La/Yb Ore-Forming Porphyries along the Qin-Hang Belt, South China. *Ore Geology Reviews*, 123: 103574. https://doi.org/10.1016/j.oregeorev.2020.103574

Rudnick, R. L., Gao, S., 2003. Composition of the Continental Crust. In: Holland, H. D., Turekian, K. K., eds., Treatise on Geochemistry, vol. 3. Elsevier-Pergamon, Oxford

Russell, S. D., Cambon, N., Pruliere, G., et al., 1987. Thyroid-Hormone Induces Precocious Expression of Fast Myosin Heavy-Chain Messenger-Rna and Protein in Rat Hindlimb Muscle. *Journal of Muscle Research and Cell Motility*, 8(1): 80–80

Russell, W. A., Papanastassiou, D. A., Tombrello, T. A., 1978. Ca Isotope Fractionation on the Earth and other Solar System Materials. *Geochimica et Cosmochimica Acta*, 42(8): 1075–1090. https://doi.org/10.1016/0016-7037(78)90105-9

Salters, V. J. M., Stracke, A., 2004. Composition of the Depleted Mantle. *Geochemistry, Geophysics, Geosystems*, 5(5): Q05B07. https://doi.org/10.1029/2003gc000597

Scherer, E., Münker, C., Mezger, K, 2001. Calibration of the Lutetium-Hafnium Clock. *Science*, 293(5530): 683–687. https://doi.org/10.1126/science.1061372

Simon, J. I., DePaolo, D. J., Moynier, F, 2009. Calcium Isotope Composition of Meteorites, Earth, and Mars. *The Astrophysical Journal Letters*, 702(1): 707–715. https://doi.org/10.1088/0004-637x/702/1/707

Steiger, R. H., Jäger, E., 1977. Subcommission on Geochronology: Convention on the Use of Decay Constants in Geo- and Cosmochronology. *Earth and Planetary Science Letters*, 36(3): 359–362. https://doi.org/10.1016/0012-821x(77)90060-7

Su, Y. P., Zheng, J. P., Griffin, W. L., et al., 2013. Petrogenesis and Geochronology of Cretaceous Adakitic, I- and A-Type Granitoids in the NE Yangtze Block: Constraints on the Eastern Subsurface

Boundary between the North and South China Blocks. *Lithos*, 175/176: 333–350. https://doi.org/10.1016/j.lithos.2013.05.016

Sun, W. D., Ding, X., Hu, Y. H., et al., 2007. The Golden Transformation of the Cretaceous Plate Subduction in the West Pacific. *Earth and Planetary Science Letters*, 262(3/4): 533–542. https://doi.org/10.1016/j.epsl.2007.08.021

Sun, W.D., Ling, M.X., Wang, F.Y., et al., 2008. Pacific Plate Subduction and Mesozoic Geological Event in Eastern China. *Bulletin of Mineralogy, Petrology and Geochemistry*, 27(3): 218–225 (in Chinese with English Abstract)

Sun, W. D., Ling, M. X., Yang, X. Y., et al., 2010. Ridge Subduction and Porphyry Copper Gold Mineralization: An Overview. *Science China (Earth Sciences)*, 53(4): 475–484. https://doi.org/10.1007/s11430-010-0024-0 (in Chinese)

Sun, W. D., Liu, L. J., Hu, Y. B., et al., 2018. Post-Ridge-Subduction Acceleration of the Indian Plate Induced by Slab Rollback. *Solid Earth Sciences*, 3(1): 1–7. https://doi.org/10.1016/j.sesci.2017.12.003

Taylor, S. R., McLennan, S. M., 1995. The Geochemical Evolution of the Continental Crust. *Reviews of Geophysics*, 33(2): 241–265. https://doi.org/10.1029/95rg00262

Wang, L. X., Ma, C. Q., Zhang, C., et al., 2018. Halogen Geochemistry of I- and A-Type Granites from Jiuhuashan Region (South China): Insights into the Elevated Fluorine in A-Type Granite. *Chemical Geology*, 478: 164–182. https://doi.org/10.1016/j.chemgeo.2017.09.033

Wang, Q., Wyman, D. A., Xu, J. F., et al., 2007. Early Cretaceous Adakitic Granites in the Northern Dabie Complex, Central China: Implications for Partial Melting and Delamination of Thickened Lower Crust. *Geochimica et Cosmochimica Acta*, 71(10): 2609–2636. https://doi.org/10.1016/j.gca.2007.03.008

Wang, W. J., 2009. Characteristics, Petrogenesis and Minerogenic Specialization of the Mesozoic Granitoids in Shitai Area, Anhui Province: [Dissertation]. Hefei University of Technology, Hefei (in Chinese with English Abstract)

Wang, Y., He, Y. S., Wu, H. J., et al., 2019. Calcium Isotope Fractionation during Crustal Melting and Magma Differentiation: Granitoid and Mineral-Pair Perspectives. *Geochimica et Cosmochimica Acta*, 259: 37–52. https://doi.org/10.1016/j.gca.2019.05.030

Weis, D., Kieffer, B., Maerschalk, C., et al., 2006. High-Precision Isotopic Characterization of USGS Reference Materials by TIMS and MC-ICP-MS. *Geochemistry, Geophysics, Geosystems*, 7(8): Q08006. https://doi.org/10.1029/2006gc001283

Wu, F. Y., Ji, W. Q., Sun, D. H., et al., 2012. Zircon U-Pb Geochronology and Hf Isotopic Compositions of the Mesozoic Granites in Southern Anhui Province, China. *Lithos*, 150: 6–25. https://doi.org/10.1016/j.lithos.2012.03.020

Xie, G. Q., Mao, J. W., Li, R. L., et al., 2008. Geochemistry and Nd-Sr Isotopic Studies of Late Mesozoic Granitoids in the Southeastern Hubei Province, Middle-Lower Yangtze River Belt, Eastern China: Petrogenesis and Tectonic Setting. *Lithos*, 104(1/2/3/4): 216–230. https://doi.org/10.1016/j.lithos.2007.12.008

Xu, X. S., Suzuki, K., Liu, L., et al., 2010. Petrogenesis and Tectonic Implications of Late Mesozoic Granites in the NE Yangtze Block, China: Further Insights from the Jiuhuashan-Qingyang Complex. *Geological Magazine*, 147(2): 219 – 232. https://doi. org/10.1017/s0016756809990367

Xue, H. M., Wang, Y. G., Ma, F., et al., 2009. Zircon U-Pb SHRIMP Ages of the Taiping (Calc-Alkaline) -Huangshan (Alkaline) Composite Intrusion: Constraints on Mesozoic Lithospheric Thinning of the Southeastern Yangtze Craton, China. *Science in China Series D: Earth Sciences*, 52: 1756 – 1770. https://doi. org/10.1007/S11430-009-0133-9 (in Chinese)

Yan, J., Chen, J. F., Xie, Z., et al., 2005. Geochemistry of Late Mesozoic Basalts from Kedoushan in the Middle and Lower Yangtze Regions: Constraints on Characteristics and Evolution of the Lithospheric Mantle. *Geochimica*, 34(5): 455–469 (in Chinese with English Abstract)

Yan, J., Liu, J. M., Li, Q. Z., et al., 2015. In Situ Zircon Hf-O Isotopic Analyses of Late Mesozoic Magmatic Rocks in the Lower Yangtze River Belt, Central Eastern China: Implications for Petrogenesis and Geodynamic Evolution. *Lithos*, 227: 57–76. https://doi. org/10.1016/j.lithos.2015.03.013

Yang, Y. Z., Wang, Y., Ye, R. S., et al., 2017. Petrology and Geochemistry of Early Cretaceous A-Type Granitoids and Late Mesozoic Mafic Dikes and Their Relationship to Adakitic Intrusions in the Lower Yangtze River Belt, Southeast China. *International Geology Review*, 59(1): 62–79. https://doi.org/10.1080/00206814.2016.1212284

Zhang, S. B., Zheng, Y. F., 2013. Formation and Evolution of Precambrian Continental Lithosphere in South China. *Gondwana Research*, 23(4): 1241–1260. https://doi.org/10.1016/j.gr.2012.09.005

Zhang, S. B., Zheng, Y. F., Wu, Y. B., et al., 2006. Zircon U-Pb Age and Hf Isotope Evidence for 3.8 Ga Crustal Remnant and Episodic Reworking of Archean Crust in South China. *Earth and Planetary Science Letters*, 252(1/2): 56–71. https://doi.org/10.1016/j.epsl.2006.09.027

Zhang, Y. S., Yan, J., Li, Q. Z., et al., 2018. Pulses of Late Mesozoic Magmatism: Zircon Ages and Hf-O Isotopic Composition of the Qingyang-Jiuhuashan Granitic Complex, Southern Anhui Province, Eastern China. *Journal of Asian Earth Sciences*, 167: 181–196. https://doi.org/10.1016/j.jseaes.2017.08.003

Zhang, Z. K., Ling, M. X., Zhang, L. P., et al., 2020. High Oxygen Fugacity Magma: Implication for the Destruction of the North China Craton. *Acta Geochimica*, 39(2): 161–171. https://doi.org/10.1007/s11631-020-00394-7

Zhu, H. L., Du, L., Li, X., et al., 2020. Calcium Isotopic Fractionation during Plate Subduction: Constraints from Back-Arc Basin Basalts. *Geochimica et Cosmochimica Acta*, 270: 379 – 393. https://doi. org/10.1016/j.gca.2019.12.004

Zhu, H. L., Zhang, Z. F., Wang, G. Q., et al., 2016. Calcium Isotopic Fractionation during Ion-Exchange Column Chemistry and Thermal Ionisation Mass Spectrometry (TIMS) Determination. *Geostandards and Geoanalytical Research*, 40(2): 185 – 194. https://doi.org/10.1111/j.1751-908x.2015.00360.x